Simulations of Luminescent Solar Concentrator Bifacial Photovoltaic Mosaic Devices Containing Four Different Organic Luminophores

Mohammadreza Aghaei, *Senior Member, IEEE*, Xitong Zhu, Michael Debije, Wallace Wong, Timothy Schmidt, and Angele Reinders, *Senior Member, IEEE*

***Abstract*—In this article, various design configurations of luminescent solar concentrator photovoltaic (LSC-PV) devices have been simulated using Monte Carlo raytracing. These LSC PV devices are composed of mono-crystalline silicon solar cells and cubical poly (methyl methacrylate) lightguides, each containing one of the following dyes: Lumogen F Red 305, Lumogen F Orange 240, Perylene Green, or Perylene-diimide di-tert-butylphenyl, which results in different device colors. In these devices, mono-crystalline silicon bifacial PV cell are placed in between the vertical edge(s) of neighboring cubical lightguides whereas monofacial PV cells are positioned at the bottom of a lightguide. Each device is made out of five cubical 10 $\times$ 10 $\times$ 10 mm^3 lightguides, meaning that the PV cells measure 10 $\times$ 10 mm^2. The main research goal of this article is to evaluate the optical and electrical performance of five of such configured LSC-PV devices. Hence, the spectral distribution of irradiance received by the edges and bottom of the devices has been simulated as well as the optical efficiency of these surfaces and the power conversion efficiency of each device. The theoretical results for power conversion efficiency are in the range of 13.3% to 18% under irradiance of 1000 W/m^2 and depend on the dyes applied. Hence, this article demonstrates the potential for energy generation by these colorful LSC-PV technologies, which we have called Mosaic devices.**

***Index Terms*—Bifacial solar cells, luminescent solar concentrator photovoltaic (LSC-PV), optical efficiency, organic luminophores, power conversion efficiency.**

Manuscript received January 17, 2022; accepted January 18, 2022. Date of publication February 16, 2022; date of current version April 21, 2022. This work was supported by the Eindhoven University of Technology (TU/e). *(Corresponding author: Mohammadreza Aghaei.)*

Mohammadreza Aghaei and Xitong Zhu are with the Department of Mechanical Engineering, Eindhoven University of Technology, 5612 AZ Eindhoven, The Netherlands (e-mail: mohammadreza.aghaei@polimi.it; x.zhu@tue.nl).

Michael Debije is with the Department of Chemical Engineering and Chemistry, Eindhoven University of Technology, 5612 AZ Eindhoven, The Netherlands (e-mail: m.g.debije@tue.nl).

Wallace Wong is with the ARC Centre of Excellence in Exciton Science, School of Chemistry, University of Melbourne, Parkville, VIC 3010, Australia (e-mail: wwhwong@unimelb.edu.au).

Timothy Schmidt is with the School of Chemistry, University of New South Wales, Sydney, NSW 2052, Australia (e-mail: timothy.schmidt@unsw.edu.au).

Angele Reinders is with the Department of Mechanical Engineering, Eindhoven University of Technology, 5612 AZ Eindhoven, The Netherlands, and also with the Department of Design, Production, and Management, University of Twente, 7522 NB Enschede, The Netherlands (e-mail: a.h.m.e.reinders@tue.nl).

This article has supplementary material provided by the authors and color versions of one or more figures available at https://doi.org/10.1109/JPHOTOV.2022.3144962.

Digital Object Identifier 10.1109/JPHOTOV.2022.3144962

I. Introduction

LUMINESCENT solar concentrator photovoltaic (LSC-PV) devices consist of transparent optical lightguides typically made of a polymer or glass containing luminophores with one or more photovoltaic (PV) solar cells mounted on one or more edges and sometimes rear of the lightguide [1], [2]. The luminophores of the LSC-PV devices absorb a fraction of the incoming irradiance, re-emitting it at usually longer wavelengths (connected downshifting). Preferably, emission takes place in spectral regions where the associated PV cells have a high external quantum efficiency. In this process photons are spectrally shifted and optically concentrated by total internal reflection to PV cells in order to be converted to electricity [3]–[8].

LSC-PV devices have shown relative insensitivity to the incidence direction of illumination, which often is a challenge for conventional PV modules [9]. Combined with other attractive features including color tunability [10], transparency, geometry flexibility, configuration versatility, and electrical interconnection invisibility [7], [11], [12], LSC-PV devices or modules could be seamlessly integrated into the urban built environment by means of building integrated PV or as smart windows for controlling the light entering room spaces [13]–[16].

Furthermore, LSC-PV technologies can be applied in such diverse applications as the automotive [17] or agricultural sectors [18], [19]: LSC-PV modules are already applied in greenhouses for combined electricity generation and spectral shifting of incoming irradiance to reddish light, which is assumed to stimulate plant growth [20], [21], or even in the production of hydrogen [22] or fine chemicals [23].

Over the past decade, there have been significant advancements and rapid growth in the field of LSCs [24]. At present, several groups in the LSC PV community are interested in bringing results obtained in the laboratory into practice by the development of small scale applications [25]–[27].

For some applications in buildings and the automotive sector, efficiencies greater than the world record of 7.1% reported by Sloof *et al.* [28] will be desirable using nontoxic colorful luminophores. Therefore, this article aims to determine the optical power efficiency (1) and power conversion efficiency (2) of LSC PV devices with an attractive mosaic geometry deploying bifacial silicon solar cells [29] based on organic

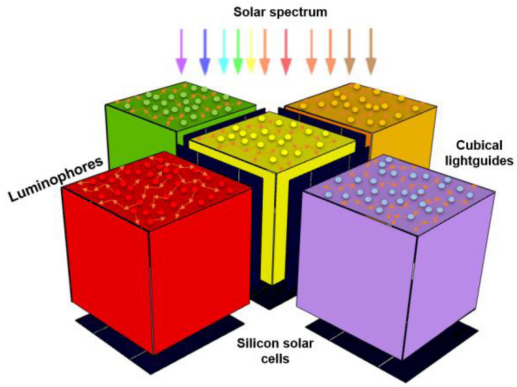

Fig. 1. Scheme of the proposed LSC-PV mosaic device, with differently colored cubical lightguides and edge-mounted bifacial and bottom-mounted monofacial PV cells.

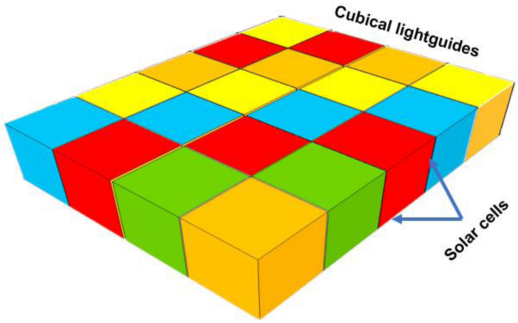

Fig. 2. Scheme of a mosaic of LSC-PV modules with differently colored interconnected devices, as shown in Fig. 1.

dyes rather than quantum dots [30]–[32] or rare earth elements [33]–[36]. In this article, we present Monte Carlo ray-tracing simulations of the optical and electrical performance of these LSC-PV mosaic devices using lightguides made of poly(methyl methacrylate) (PMMA) doped with a variety of perylene dyes including Lumogen F Red 305 (LR 305), Lumogen F Orange 240 (LO 240), Perylene Green (PG), and perylene-diimide (PDI) di-tert-butylphenyl (bPDI-3).

In these devices mono-crystalline silicon bifacial and monofacial solar cells (mono c-Si) are mounted on the edges and bottom of cubical lightguides, which when attached, collectively form an array of lightguides with bifacial solar cells between them and monofacial solar cells at their rears. Thus, four $10 \times 10 \times 10\,\mathrm{mm}^3$ lightguides are adhered each by one edge to a central lightguide by four bifacial solar cells, see Fig. 1. Various modifications of this design configuration have been explored using cubical lightguides containing different luminophores in a variety of colors. This concept can be developed with customization of geometry in a scalable device, see Fig. 2.

II. Materials and Methods

A. Materials and Simulation Set Up

In this simulation study, PMMA was used as the host material as an inexpensive and easily processable material, widely

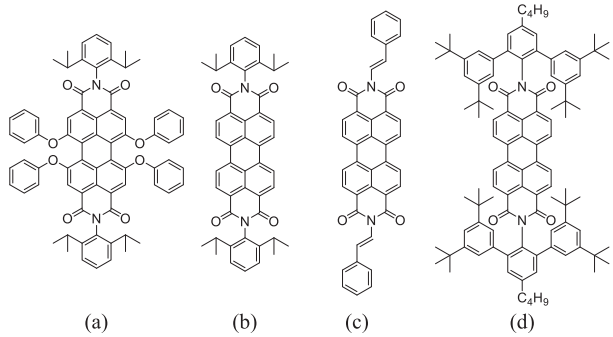

Fig. 3. Molecular structures of (a) LFR 305, (b) LFO 240, (c) PG, and (d) bPDI-3.

TABLE I
Electrical Characteristics of the Bifacial Silicon Solar Cells

Voc (V)	Jsc (mA/cm^2)	Vmpp (V)	Jmpp (mA/cm^2)	Pmax (W)	Efficiency (front) (%)	Bifaciality (%)
0.66	39	0.56	37	5.13	21	87

employed for LSCs. It has excellent transparency to visible light with a refractive index of 1.49 at 589 nm, as well as good compatibility with the organic luminescent materials used [37]. The PMMA was doped with one of four organic dyes, namely LR 305, LO 240, PG, or PDI-3 (see Fig. 3 for the chemical structures of the luminophores). The edge-mounted bifacial silicon solar cells (with a refractive index of $n_{\mathrm{PV}} = 3.4$ at 550 nm) were modeled as receiver planes to convert the waveguided photons into electricity: Table I summarizes the electrical characterization of the bifacial silicon solar cells.

LR 305 and LO 240 dyes (BASF) have close-to-unity photoluminescence quantum yields (PLQY), around 95%, and good photostability under ultraviolet (UV) and visible lights [38], [39]. The PG dye has a large Stokes shift (98 nm) but relatively low PLQY (26%) [40]. The bPDI-3 fluorophore is a promising derivative of perylene diimide (PDI) with a PLQY of 98% [41]–[43]. Fig. 4 shows the absorption and photoluminescence spectra curves of the luminophores. The Stokes shifts of the red, orange, green, and bPDI-3 dyes were, respectively, 27, 7, 98, and 9 nm.

In the simulation, we calculated the mean free path (MFP) for the bPDI-3 luminophore using the Beer–Lambert law and the wavelength-dependent optical cross-section as well as molar absorptivity coefficient (see Supporting Information, part A). The optical cross-section of other luminophores were obtained via measurement at The Netherlands Organization for Applied Scientific Research (TNO) and the MFP values were computed at different concentrations accordingly (see Supporting Information, part B). The MFP is defined as the average distance that a photon can travel freely without being scattered or absorbed by luminescent particles. This photon-luminophore interaction is more likely to occur at higher concentration of the luminophores, resulting in shorter MFPs [44], [45].

TABLE II
CONFIGURATION OF SIMULATED LSC-PV DEVICES. ALL DEVICES USED $10 \times 10 \times 10$ MM^3 LIGHTGUIDES, FOUR 10×10 MM^2 EDGE-MOUNTED SI PV CELLS AND FIVE BOTTOM-MOUNTED PV CELLS

LSC-PV device	Number of cubical LSCs	Host material	Luminescent materials
1	5	PMMA	LR 305
2	5	PMMA	LO 240
3	5	PMMA	bPDI-3
4	5	PMMA	PG
5	5	PMMA	LR 305, LO 240, 3-bPDI, and PG (1 cube each)

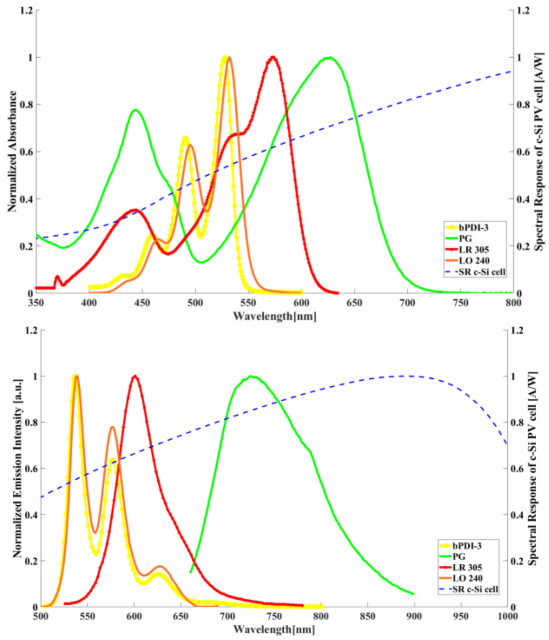

Fig. 4. UV-vis absorption (top) and photoluminescence (bottom) spectra of LR 305 (red line), LO 240 (orange line), PG (green line), and bPDI-3 (yellow line) versus the normalized spectral response curve of the silicon solar cell (dashed blue line).

The properties of the lightguides and solar cells were imported into the commercially available LightTools (Synopsys) software for ray-tracing simulations [29], considering absorption, refraction, reflection, dye emission, and transmission. LightTools is a 3-D design and optical engineering software, which can support complex ray-tracing simulations, optimization, visual prototyping, and can generate photorealistic renderings of illumination applications [46], and was used due to its ability to handle complex 3-D geometries and simulate the LSC-PV devices under standard test conditions (STC), which are defined by an irradiance of 1000 W/m^2 with an AM 1.5 spectrum and a cell temperature of 25 °C. Monte Carlo ray-tracing has previously proven to be useful for predicting performance of LSC-PV devices [47]. For this article, incident photons were traced from their entry into a cubical LSC-PV device until lost from the system or collected by the attached bifacial solar cells [48].

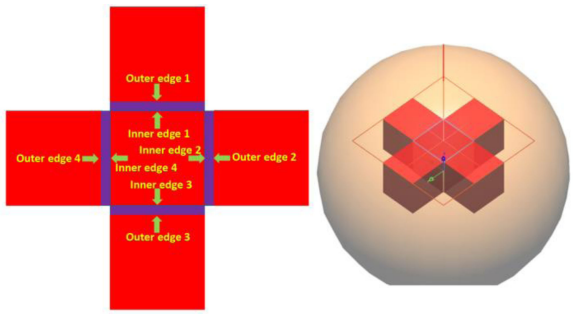

Fig. 5. Three-dimensional geometry model of cubical LSC-PV with edge- and bottom-mounted bifacial PV cells, Left: top view of a unit cell of this device with neighboring lightguides; Right: model in LightTools; the orange sphere shows the diffuse irradiance and the red line indicates the direction of the direct beam irradiance.

B. Design Configuration

We designed and modeled five different mosaic LSC-PV devices based on five cubical lightguides containing different luminescent materials and number of bifacial silicon PV cells mounted on the edges and/or bottom sides of the lightguides: see Table II for a list of configurations. An example configuration is depicted in Fig. 5, see also [29]. Five cubical LSCs and their bifacial solar cells are attached around a single cubical lightguide. In this concept, the PV cells also were mounted on the bottom side of cubical LSCs to maximize the device efficiency.

C. Simulation Assumptions

In this simulation study, we assumed the following.

1) The organic luminophores have a high quality and photostability with constant quantum yield over the entire wavelength range.
2) Luminophores have good solubility in the host-matrix material (PMMA).
3) Ideal optical interfaces between host matrix material and PV cells without any irradiance losses.
4) PV cells with efficiency of 21% without any defects or reflection losses.
5) An ideal aperture surface without structures that could scatter incoming irradiance back to the surroundings as well as ideal transmission.

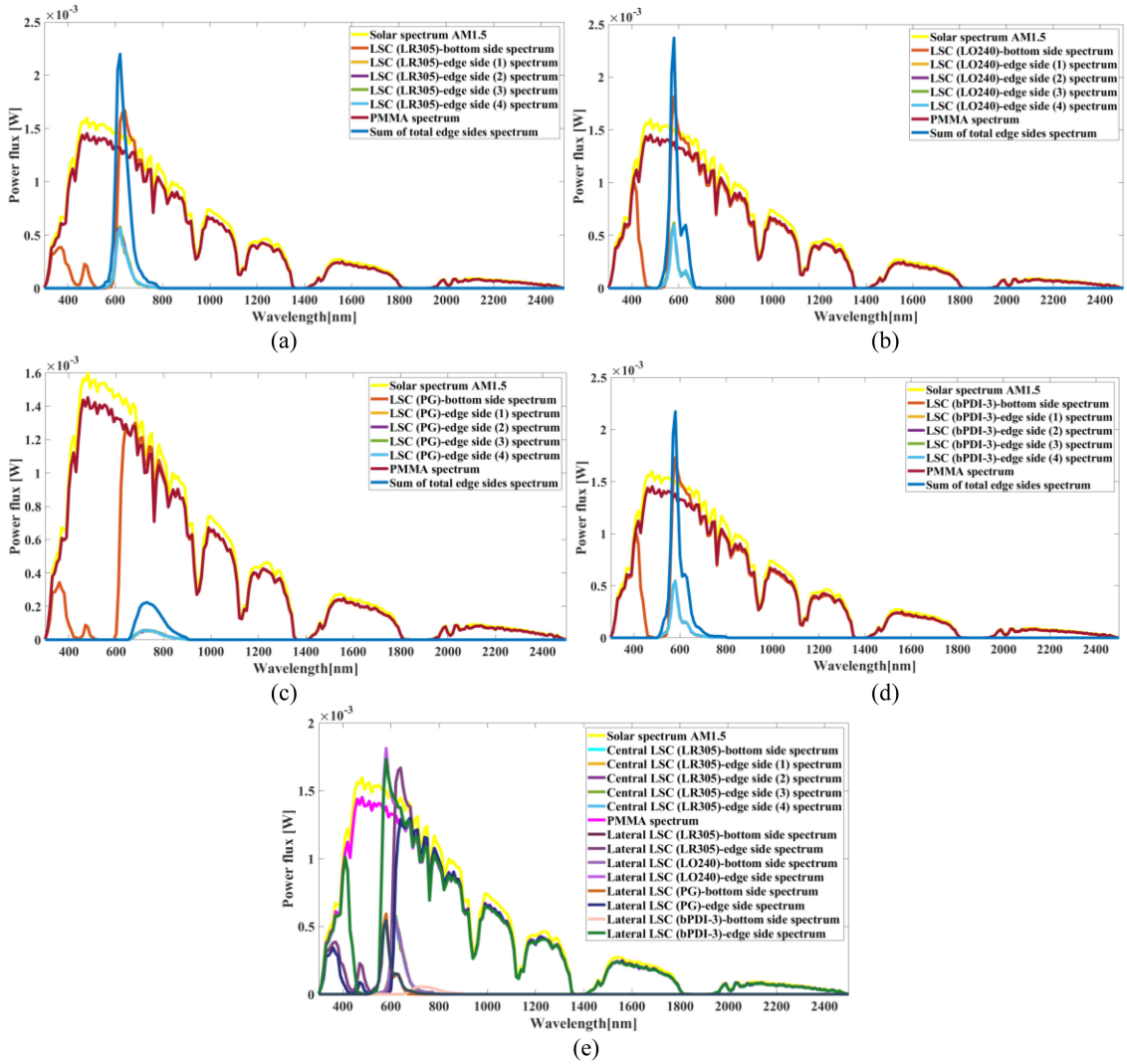

Fig. 6. Spectrum distribution at the edges and bottom sides of the LSCs in: (a) device 1, (b) device 2, (c) device 3, (d) device 4, and (e) device 5, compared to the solar spectrum (AM 1.5G) received by the top surface of the lightguides.

III. Results

The simulation assumed incident light could only enter the lightguide via the top surface: the sides were effectively "masked" for purposes of this article. Please notice that in an actual device, of course, the light would be capable of entering through the unadorned edges of the outer cubes. Fig. 6 depicts the spectral distribution generated at the lightguide edges and passing through the bottom of the cubical lightguides at the middle of the emission faces, and the solar spectrum (AM 1.5) received by the top surface of LSCs. In addition, the spectrum distribution passing through the bottom side of a simulated clear PMMA is also shown in this figure.

The spectral irradiance at the bottom of the cubical LSCs containing LR 305 and LO 240 dyes naturally contain less power for wavelengths in the absorption range of the embedded dyes but produce a higher power flux around 650 nm and 580 nm, respectively, the emission range of the dyes. In contrast, the LSCs containing PG and bPDI-3 supply a reduced power to the bottom cell even at their peak emission wavelengths, likely a result of their lower FQYs. The edge-mounted bifacial cells show power flux corresponding to the range of dyes' emission peak, as nonscattering lightguides are assumed.

The optical power efficiency, η_{PE}, of the cubical LSCs is calculated using the resulting data of raytracing simulation through

$$\eta_{\mathrm{OE}} = \frac{\sum G_{\mathrm{PV}}}{G_{in}} \tag{1}$$

where G_{PV} the irradiance on both surfaces of the bifacial PV cells in (W/m^2) and G_{in} is the incident solar irradiance on the aperture area of the cubical LSC-PV device in (W/m^2). As the spectral composition incident to the PV is different from the original solar spectrum, it is necessary to use the spectral response to calculate the power production of LSC PV devices.

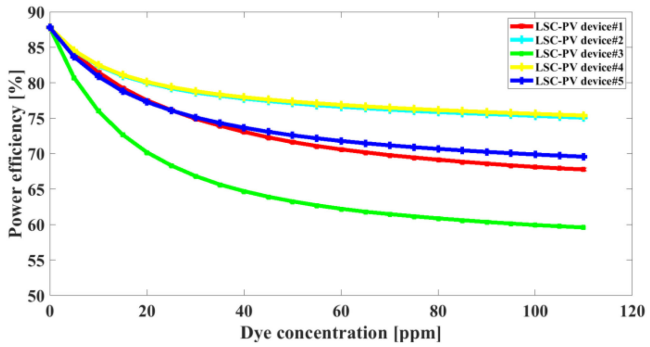

Fig. 7. Comparison of power efficiency of the LSC-PV devices as a function of the dye concentration.

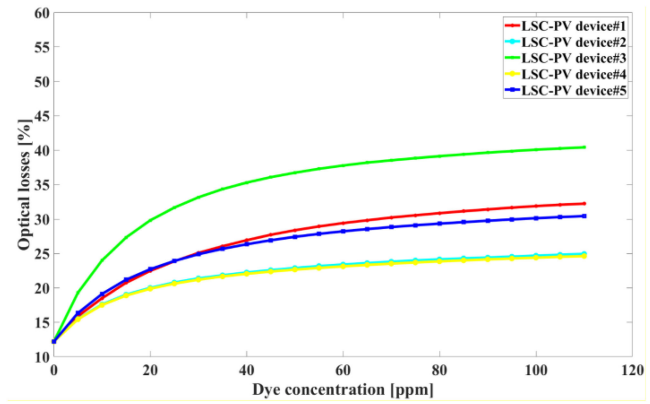

Fig. 8. Optical losses in the LSC-PV devices as function of the dye concentration.

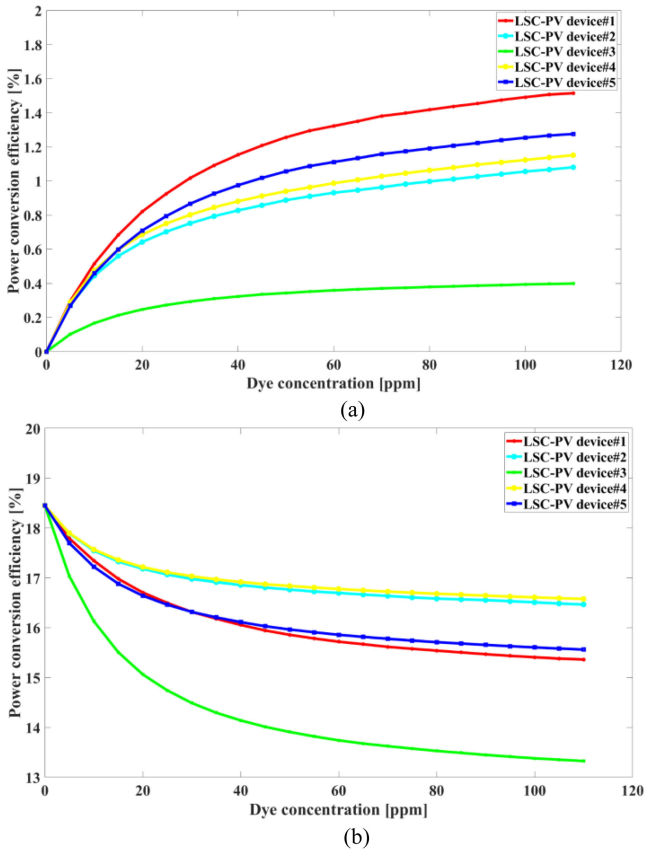

Fig. 9. Power conversion efficiency of the LSC PV devices as a function of the dye concentration: (top) with only edges-mounted bifacial PV cells, and (bottom) the device with edges- and bottom-mounted bifacial PV cells.

The power conversion efficiency (PCE) of an LSC PV device η_{dev} [7] is calculated via

$$\eta_{dev} = \frac{\sum_{i=1}^{n} \int_{\lambda=0}^{4500\ \mathrm{nm}} S^{i}_{\mathrm{PV}}(\lambda)\, SR(\lambda)\, \mathrm{FF} \mathrm{V}_{\mathrm{oc}} A^{i}_{\mathrm{PV}} d\lambda}{\int_{0}^{\infty} S_{ap}(\lambda)\, A_{ap} d\lambda}. \quad (2)$$

Fig. 7 displays the simulated optical efficiency of the LSC-PV devices as a function of the dye concentration when exposed to STC with 70% direct and 30% diffuse irradiance. The optical efficiency at the edges and bottom of the lightguide of cubical LSCs decreases with increasing dye concentration because higher dye concentrations result in increased reabsorption losses due to the overlap of the absorption and emission spectra of the dyes. Device 4, with the larger Stokes shift bPDI-3 dye showed a generally higher optical performance under all dye concentrations.

Fig. 8 depicts the simulated power losses of the LSC-PV devices as a function of dye concentration. The losses stem from the limited PLQY of the dyes, emission and/or re-emission of light outside the "capture cone" of the lightguide, and lightguide absorption, all of which can influence negatively on the performance of LSC-PV devices.

The PCE of the LSC-PV devices were calculated according to (2) and are presented in Fig. 9(left), which shows the PCE of the devices with only edge-mounted bifacial solar cells increases with the concentration of LF 305, LO 240, PG, bPDI-3 dyes, whereas the PCE of LSC-PV devices with edge- and bottom-mounted bifacial PV cells decreases smoothly with the increase of the dye concentration, see Fig. 9(right).

The two figures can be explained by the increase in incident dye-emitted irradiance on the edge-mounted PV cells and a decrease in the incident solar irradiance on the bottom-mounted solar cells with increasing dye concentration. While the increase in dye concentration led to an increase in irradiance for the solar cells attached on the edges, given that the dye quantum yields and emitted light transport are not 100% efficient, there is a significant decrease in the incident irradiance for the PV cells placed on the bottom sides of lightguides.

Table III summarizes the optical and electrical efficiencies of cubical bifacial LSC-PV devices with different luminophores obtained through ray tracing simulation: the highest power efficiency of 84.6% and power conversion efficiency of 18% (at 5 ppm) were obtained for the LSC-PV device 4 under STC with a 70% share of direct irradiance and 30% share of diffuse irradiance.

We performed preliminary investigations on the effect of dimensional variations of these cubical LSCs and PV on the performance of LSC-PV devices, see Fig. 10. According to our observations, an increase in the dimensions of cubical lightguides and the size of solar cells led to a slight decrease

TABLE III
POWER EFFICIENCY AND POWER CONVERSION EFFICIENCY OF BIFACIAL LSC-PV DEVICES

LSC-PV device	Power efficiency of full device (%)		PCE of device with edge-mounted bifacial cells (%)		PCE of full device (%)	
	Max	Min	Max	Min	Max	Min
1	84.1	67.8	1.5	0.3	17.8	15.4
2	84.5	75.1	1.1	0.27	17.9	16.5
3	80.7	59.6	0.4	0.1	17	13.3
4	84.6	75.4	1.2	0.3	18	16.6
5	83.7	69.6	1.3	0.26	17.7	15.6

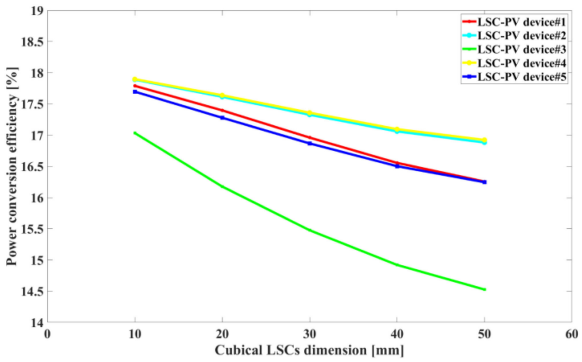

Fig. 10. Power conversion efficiency of the LSC PV devices as a function of the dimensional variation of cubical lightguides at the concentrations of 5 ppm.

in the PCE of devices, mainly due to increased probability of reabsorption events.

IV. DISCUSSION AND CONCLUSIONS

In this article, we have shown a novel mosaic configuration for LSC-PV devices using colorful cubical lightguides made of PMMA containing four different organic fluorophores; LR 305, LO 240, PG, and bPDI-3. Mono c-Si solar cells were located between the lightguides and mounted on the bottom sides of the lightguides to convert the incident unabsorbed irradiance into electricity. We have configured five LSC-PV devices to evaluate their optical performance and electrical performance by using Monte Carlo ray tracing simulations executed in LightTools software.

The spectral distribution of irradiance on the edges and bottom sides of the devices was investigated, as well as the electrical power production of these LSC PV devices. According to the ray tracing simulations, the theoretical power conversion efficiency under ideal circumstances is in the range of 13.3% to 18% at irradiance of 1000 W/m^2 and depend on the dyes applied. The highest optical power efficiency of 84.6% and PCE of 18% were obtained for the LSC device consisting of five cubical lightguide ($10 \times 10 \times 10$ mm^3) containing bPDI-3 dye at 5 ppm, with 4 edge- and 5 bottom-mounted bifacial solar cells. Hence, this article demonstrates the potential for energy generation by this new type of LSC PV devices.

While the system efficiency is lower than the silicon PV cells alone, the LSC performance is considerably greater than the moderate efficiencies reported in the literature. But the reader should be aware of the fact that the primary goals of LSC-PV devices is not to compete with the efficiency of conventional solar PV modules, because their customizable design features, such as color, transparency, and shape, are prevailing for integration purposes. Once a simple assembly technique is created, these mosaic-LSC devices could allow for intricate, high-efficiency devices with a high degree of artistic beauty. It is anticipated that this device could find application in higher-end applications requiring greater efficiency where aesthetics is also of utmost importance, allowing some leeway for the additional costs required to produce these specialized systems.

ACKNOWLEDGMENT

The authors would like to acknowledge their discussions with Dr. L. Slooff Hoek from TNO and Dr. G. Timmermans from TU/e in preparing the input parameters of the LSC devices.

REFERENCES

[1] M. Rafiee, S. Chandra, H. Ahmed, and S. J. McCormack, "An overview of various configurations of luminescent solar concentrators for photovoltaic applications," *Opt. Mater. (Amst)*, vol. 91, pp. 212–227, 2019, doi: 10.1016/j.optmat.2019.01.007.

[2] M. J. Currie, J. K. Mapel, T. D. Heidel, S. Goffri, and M. A. Baldo, "High-efficiency organic solar concentrators for photovoltaics," *Science (80-.)*, vol. 321, no. 5886, pp. 226–228, Jul. 2008, doi: 10.1126/science.1158342.

[3] M. G. Debije and P. P. C. Verbunt, "Thirty years of luminescent solar concentrator research: Solar energy for the built environment," *Adv. Energy Mater.*, vol. 2, no. 1. pp. 12–35, Jan. 2012, doi: 10.1002/aenm.201100554.

[4] W. G. J. H. M. van Sark *et al.*, "Luminescent solar concentrators–A review of recent results," *Opt. Exp.*, vol. 16, no. 26, Dec. 2008, Art. no. 21773, doi: 10.1364/oe.16.021773.

[5] F. Meinardi *et al.*, "Large-area luminescent solar concentrators based on Stokes-shift-engineered nanocrystals in a mass-polymerized PMMA matrix," *Nat. Photon.*, vol. 8, pp. 392–399, 2014, doi: 10.1038/nphoton.2014.54.

[6] A. Goetzberger and W. Greube, "Solar energy conversion with fluorescent collectors," *Appl. Phys.*, vol. 14, pp. 123–139, 1977, doi: 10.1007/BF00883080.

[7] M. G. Debije, R. C. Evans, and G. Griffini, "Laboratory protocols for measuring and reporting the performance of luminescent solar concentrators," *Energy Environ. Sci*, vol. 14, pp. 293–301, 2021, doi: 10.1039/d0ee02967j.

[8] B. McKenna and R. C. Evans, "Towards efficient spectral converters through materials design for luminescent solar devices," *Adv. Mater.*, vol. 29, no. 28, 2017, Art. no. 1606491.

[9] M. G. Debije and V. A. Rajkumar, "Direct versus indirect illumination of a prototype luminescent solar concentrator," *Sol. Energy*, vol. 122, pp. 334–340, 2015.

[10] G. H. Timmermans, B. W. H. Saes, and M. G. Debije, "Dual-responsive 'smart' window and visually attractive coating based on a diarylethene photochromic dye," *Appl. Opt.*, vol. 58, no. 36, pp. 9823–9828, 2019.

[11] A. Reinders, R. Kishore, L. Slooff, and W. Eggink, "Luminescent solar concentrator photovoltaic designs," *Jpn. J. Appl. Phys.*, vol. 57, no. 8, 2018, doi: 10.7567/JJAP.57.08RD10.

[12] M. G. Debije, C. Tzikas, V. A. Rajkumar, and M. M. de Jong, "The solar noise barrier project: 2. The effect of street art on performance of a large scale luminescent solar concentrator prototype," *Renewable Energy*, vol. 113, pp. 1288–1292, 2017.

[13] G. H. Timmermans, R. F. Douma, J. Lin, and M. G. Debije, "Dual thermal-/electrical-responsive luminescent 'Smart'Window," *Appl. Sci.*, vol. 10, no. 4, 2020, Art. no. 1421.

[14] J. A. H. P. Sol, G. H. Timmermans, A. J. van Breugel, A. P. H. J. Schenning, and M. G. Debije, "Multistate luminescent solar concentrator 'Smart' windows," *Adv. Energy Mater.*, vol. 8, no. 12, p. 1702922, Apr. 2018, doi: 10.1002/aenm.201702922.

[15] M. G. Debije, "Solar energy collectors with tunable transmission," *Adv. Funct. Mater.*, vol. 20, no. 9, pp. 1498–1502, 2010.

[16] Y. Zhao and R. R. Lunt, "Transparent luminescent solar concentrators for large-area solar windows enabled by massive stokes-shift nanocluster phosphors," *Adv. Energy Mater.*, vol. 3, no. 9, pp. 1143–1148, 2013.

[17] C. Ding, H. Li, W. Zheng, Y. Wang, N. Chang, and X. Lin, "Luminescent solar concentrator-based photovoltaic reconfiguration for hybrid and plug-in electric vehicles," in *Proc. IEEE 34th Int. Conf. Comput. Des*., 2016, pp. 281–288.

[18] G. H. Timmermans *et al.*, "Advanced optical materials for sunlight control in greenhouses," *Adv. Opt. Mater.*, vol. 8, no. 18, 2020, Art. no. 2000738.

[19] C. Corrado *et al.*, "Power generation study of luminescent solar concentrator greenhouse," *J. Renewable Sustain. Energy*, vol. 8, no. 4, Jul. 2016, doi: 10.1063/1.4958735.

[20] S. M. El-Bashir and A. A. Al-Jaghwani, "Perylene-doped polycarbonate coatings for acrylic active greenhouse luminescent solar concentrator dryers," *Results Phys,* vol. 16, 2020, Art. no. 102920.

[21] M. E. Loik *et al.*, "Wavelength-Selective solar photovoltaic systems: Powering greenhouses for plant growth at the food-energy-water nexus," *Earth's Future*, vol. 5, no. 10, pp. 1044–1053, 2017, doi: 10.1002/2016EF000531.

[22] G. Panzeri, E. Tatsi, G. Griffini, and L. Magagnin, "Luminescent solar concentrators for photoelectrochemical water splitting," *ACS Appl. Energy Mater.*, vol. 3, no. 2, pp. 1665–1671, 2020.

[23] D. Cambié *et al.*, "Energy-efficient solar photochemistry with luminescent solar concentrator based photomicroreactors," *Angew. Chemie*, vol. 131, no. 40, pp. 14512–14516, 2019.

[24] R. Mazzaro and A. Vomiero, "The renaissance of luminescent solar concentrators: The role of inorganic nanomaterials," *Adv. Energy Mater.*, vol. 8, no. 33, 2018, Art. no. 1801903.

[25] W. van Sark *et al.*, "The 'electric mondrian' as a luminescent solar concentrator demonstrator case study," *Sol. RRL*, vol. 1, no. 3/4, 2017, Art. no. 1600015.

[26] A. Kerrouche, D. A. Hardy, D. Ross, and B. S. Richards, "Luminescent solar concentrators: From experimental validation of 3D ray-tracing simulations to coloured stained-glass windows for BIPV," *Sol. Energy Mater. Sol. Cells*, vol. 122, pp. 99–106, 2014, doi: 10.1016/j.solmat.2013.11.026.

[27] Á. Bognár *et al.*, "The solar noise barrier project 4: Modeling of full-scale luminescent solar concentrator noise barrier panels," *Renewable Energy*, vol. 151, pp. 1141–1149, 2020.

[28] L. H. Slooff *et al.*, "A luminescent solar concentrator with 7.1% power conversion efficiency," *Phys. Status Solidi - Rapid Res. Lett.*, vol. 2, no. 6, pp. 257–259, Dec. 2008, doi: 10.1002/pssr.200802186.

[29] M. Aghaei, M. Nitti, N. J. Ekins-Daukes, and A. H. M. E. Reinders, "Simulation of a novel configuration for luminescent solar concentrator photovoltaic devices using bifacial silicon solar cells," *Appl. Sci.*, vol. 10, p. 871, 2020, doi: 10.3390/app10030871.

[30] E. Oh *et al.*, "Meta-analysis of cellular toxicity for cadmium-containing quantum dots," *Nat. Nanotechnol.*, vol. 11, no. 5, 2016, Art. no. 479.

[31] R. Hardman, "A toxicologic review of quantum dots: Toxicity depends on physicochemical and environmental factors," *Environ. Health Perspect.*, vol. 114, no. 2, pp. 165–172, 2006.

[32] T. Wu and M. Tang, "Toxicity of quantum dots on respiratory system," *Inhalation Toxicol.*, vol. 26, no. 2, pp. 128–139, 2014.

[33] H. Zhang *et al.*, "Chronic toxicity of rare-earth elements on human beings," *Biol. Trace Element Res.*, vol. 73, no. 1, pp. 1–17, 2000.

[34] G. Pagano, M. Guida, F. Tommasi, and R. Oral, "Health effects and toxicity mechanisms of rare earth elements—Knowledge gaps and research prospects," *Ecotoxicol. Environ. Saf.*, vol. 115, pp. 40–48, 2015.

[35] N. Malhotra *et al.*, "An updated review of toxicity effect of the rare earth elements (REEs) on aquatic organisms," *Animals*, vol. 10, no. 9, 2020, Art. no. 1663.

[36] S. A. Abdelnour *et al.*, "Impacts of rare earth elements on animal health and production: Highlights of cerium and lanthanum," *Sci. Total Environ.*, vol. 672, pp. 1021–1032, 2019.

[37] M. Zettl, O. Mayer, E. Klampaftis, and B. S. Richards, "Investigation of host polymers for luminescent solar concentrators," *Energy Technol,* vol. 5, no. 7, pp. 1037–1044, 2017.

[38] L. R. Wilson and B. S. Richards, "Measurement method for photoluminescent quantum yields of fluorescent organic dyes in polymethyl methacrylate for luminescent solar concentrators," *Appl. Opt.*, vol. 48, no. 2, pp. 212–220, 2009.

[39] G. Seybold and G. Wagenblast, "New perylene and violanthrone dyestuffs for fluorescent collectors," *Dyes Pigments*, vol. 11, no. 4, pp. 303–317, 1989.

[40] D. Aigner, S. M. Borisov, P. Petritsch, and I. Klimant, "Novel near infra-red fluorescent pH sensors based on 1-aminoperylene bisimides covalently grafted onto poly (acryloylmorpholine)," *Chem. Commun.*, vol. 49, no. 21, pp. 2139–2141, 2013.

[41] R. P. Sabatini *et al.*, "Molecularly isolated perylene diimides enable both strong exciton–photon coupling and high photoluminescence quantum yield," *J. Mater. Chem. C*, vol. 7, no. 10, pp. 2954–2960, 2019.

[42] B. Zhang *et al.*, "Highly fluorescent molecularly insulated perylene diimides: Effect of concentration on photophysical properties," *Chem. Mater.*, vol. 29, no. 19, pp. 8395–8403, 2017.

[43] R. P. Sabatini *et al.*, "Organic polariton lasing with molecularly isolated perylene diimides," *Appl. Phys. Lett.*, vol. 117, no. 4, 2020, Art. no. 41103.

[44] L. M. Chávez, "Optimization of a luminescent solar concentrator," M.S. thesis, Delft Univ. Technol., Delft, The Netherlands, 2017, pp. 12–38. [Online]. Available: http://resolver.tudelft.nl/uuid:832a9936-4817-4fbc-a677-234337db68d9

[45] K. Busch, C. M. Soukoulis, and E. N. Economou, "Transport and scattering mean free paths of classical waves," *Phys. Rev. B*, vol. 50, no. 1, 1994, Art. no. 93.

[46] synopsys, "LightTools illumination design software," Accessed: Mar. 2021. [Online]. Available: https://www.synopsys.com/optical-solutions/lighttools.html

[47] S. R. Wilton, "Monte Carlo ray-tracing simulation for optimizing luminescent solar concentrators," M.S. thesis, PennState, 2012, pp. 28–57. [Online]. Available: https://etda.libraries.psu.edu/catalog/13856

[48] J. Shu *et al.*, "Monte-Carlo simulations of optical efficiency in luminescent solar concentrators based on all-inorganic perovskite quantum dots," *Phys. B Condens. Matter*, vol. 548, no. June, pp. 53–57, 2018, doi: 10.1016/j.physb.2018.08.021.